COVID-19 Treatments and Pathogenesis Including Anosmia in K18-hACE2 mice

Jian Zheng[1,#], **Lok-Yin Roy Wong**[1,#], **Kun Li**[2,#], **Abhishek Kumar Verma**[1,#], **Miguel Ortiz**[2], **Christine Wohlford-Lenane**[2], **Mariah R. Leidinger**[3], **C. Michael Knudson**[3], **David K. Meyerholz**[3], **Paul B. McCray Jr.**[1,2,*], **Stanley Perlman**[1,2,*]

[1]Department of Microbiology and Immunology, University of Iowa, Iowa City, Iowa, USA

[2]Department of Pediatrics, University of Iowa, Iowa City, Iowa, USA

[3]Department of Pathology, University of Iowa, Iowa City, Iowa, USA

Abstract

The ongoing COVID-19 pandemic is associated with substantial morbidity and mortality. While much has been learned in the first months of the pandemic, many features of COVID-19 pathogenesis remain to be determined. For example, anosmia is a common presentation and many patients with this finding show no or only minor respiratory signs[1]. Studies in animals experimentally infected with SARS-CoV-2, the cause of COVID-19, provide opportunities to study aspects of the disease not easily investigated in human patients. While COVID-19 severity ranges from asymptomatic to lethal[2], most experimental infections provide insights into mild disease[3]. Here, using K18-hACE2 mice that we originally developed for SARS studies[4], we show that infection with SARS-CoV-2 causes severe disease in the lung, and in some mice, the brain. Evidence of thrombosis and vasculitis was detected in mice with severe pneumonia. Further, we show that infusion of convalescent plasma (CP) from a recovered COVID-19 patient protected against lethal disease. Mice developed anosmia at early times after infection. Notably, while pretreatment with CP prevented significant clinical disease, it did not prevent anosmia. Thus K18-hACE2 mice provide a useful model for studying the pathological underpinnings of both mild and lethal COVID-19 and for assessing therapeutic interventions.

Keywords

---

*Correspondence and requests for materials should be addressed to: Stanley Perlman (stanley-perlman@uiowa.edu) or Paul B. McCray, Jr. (paul-mccray@uiowa.edu).
#Contributed equally to this manuscript

SARS-CoV-2 uses the same receptor as SARS-CoV, human angiotensin-converting enzyme 2, (hACE2)[5]. Mice, which are SARS-CoV-susceptible, are resistant to infection with SARS-CoV-2 because of incompatibilities between mouse ACE2 and the viral spike protein. During the 2003-2004 SARS epidemic, since infected mice developed only mild disease, we and others engineered mice that transgenically displayed hACE2[4,6,7]. K18-hACE2 mice express hACE2 driven by the cytokeratin 18 promoter, predominantly in epithelial cells[8]. SARS-CoV-infected-K18-hACE2 mice developed overwhelming encephalitis, and mild virus-induced pneumonia[4]. Both SARS-CoV-2 and SARS-CoV use hACE2 but show differences in disease manifestations in patients. SARS-CoV-2 infects the upper airways to a greater extent than SARS-CoV and, further, has been associated with clinical manifestations such as anosmia, ageusia, thrombosis and endothelial damage in the lung vasculature, cardiac and neurological disease, and a multisystem inflammatory disease in children and adolescents[1,9,10]. Based on these observations, we reasoned that SARS-CoV-2 infection of the K18-hACE2 mice might also show differences in pathogenesis. Here we demonstrate the utility of K18-hACE2 mice for studies of COVID-19 disease and treatments.

Clinical and virological characterization.

To assess the susceptibility of K18-hACE2 mice to SARS-CoV-2, we intranasally challenged male and female animals using inocula of 10^3, 10^4, and 10^5 PFU. We observed a dose-dependent increase in weight loss and mortality (Fig. 1a). At the 10^5 PFU inoculum, all animals succumbed, while all mice survived when challenged with 10^3 PFU. There was variable mortality when mice were inoculated with 10^4 PFU (2/3 female and 3/7 male mice survived). To better understand the cause(s) of this morbidity and mortality, we assessed the tissue distribution of infectious virus and viral genomic RNA at 2, 4, and 6 days post infection (dpi) in animals receiving 10^5 PFU SARS-CoV-2. The predominant target organs were the lung at early timepoints, and variably, the brain at later timepoints. Virus replicated to high titers in lung tissue at 2 dpi and decreased at 4 and 6 dpi (Fig. 1b). In some, but not all animals, brain titers gradually increased from 2 to 6 dpi. Variability in brain infection was also described in a recent study of SARS-CoV-2-infected K18-hACE2 mice[11]. Small amounts of infectious virus were detected in the kidney, small intestine, and colon, perhaps signifying low level hematogenous dissemination (Fig. 1b). We also detected viral RNA in heart, liver, spleen, kidney, intestine, and colon (Extended Data Fig. 1a). These results demonstrate that SARS-CoV-2 infection of K18-hACE2 mice causes a dose-dependent lethal respiratory illness, with a subset of animals developing brain infection that also contributes to death.

Extensive and progressive lung disease.

In view of the early pulmonary virus replication, we stained lungs at 4 and 6 dpi for SARS-CoV-2 antigen. Using an inoculum of 10^5 PFU, we observed extensive and diffuse parenchymal localization of SARS-CoV-2 nucleocapsid (N) protein at 4 dpi that was less intense by 6 dpi (Extended Data Fig. 1b). Uninfected tissues showed no N protein signal. Examination of hematoxylin and eosin stained tissues revealed evidence of diffuse alveolar damage with progressive alveolar/interstitial lesions characterized by edema, inflammation, and focal cytomegaly in some alveolar lining cells (Extended Data Fig. 1c). Also observed

was an accumulation of immune effector cells, including granulocytes and macrophages, evidence of cell death, hemorrhage, hyaline membranes, occasional vascular thrombi (Extended Data Fig. 1c), and rare syncytia. Pulmonary vascular thrombi are often observed in severe human COVID-19[9]. These findings are summarized in Extended Data Fig. 1d.

We also surveyed liver, heart, spleen, kidney, small intestine, and colon tissues for disease-associated changes (Extended Data Fig. 2). At 4 dpi, occasional vessels in the liver had evidence of fibrin thrombi adherent along the vascular wall (Extended Data Fig. 2a), suggestive of the coagulopathy observed in COVID-19 autopsies[12]. The other tissues examined showed no disease-specific changes. To further characterize the lung tissue responses to SARS-CoV-2 infection, we assessed the expression of several cytokines, chemokines, and innate immune transcripts at 2, 4, and 6 dpi by qRT PCR. As shown in Extended Data Fig. 3a, there were significant increases in type I, II, and III interferons, ISG-15, RIG-I, MDA5, IL-1β, IL-6, IL-8, IL-12, CCL-2, CCL-5, CCR7, CXCL-2, CXCL-9, CXCL-10, and TNF compared to uninfected lungs over the course of infection. Similar changes in pro-inflammatory molecule expression were observed in COVID-19 patients[13].

Inflammatory cell infiltration

To further investigate the factors contributing to lung injury and virus clearance, we performed immunophenotyping of infiltrating cells at 4 and 6 dpi (Extended Data Fig. 3b-e). We observed a progressive increase in the numbers of macrophages and monocytes, neutrophils, and CD4 and CD8 T cells (Extended Data Fig. 3e). Infiltrating inflammatory macrophage/monocytes and neutrophils may have both protective and pathogenic roles, based on previous studies of SARS and MERS[14]. Virus-specific CD8 and CD4 T cells, which are required for optimal SARS-CoV-2 clearance, were detected in lungs at 6 dpi. These cells responded to peptide pools representing SARS-CoV-2 S, N, and M proteins to varying extents, as assessed by IFN-γ and TNF expression (Extended Data Fig. 3c, d). Together these results indicate that lung disease in K18-hACE2 mice shares features with severe COVID-19. Another characteristic of severe human COVID-19 is an early antibody response, consistent with plasmablast activation[13]. We detected serum neutralizing antibodies as early as 6 dpi, consistent with such a response (Extended Data Fig. 3f).

Brain infection in some mice.

Since infectious virus was detected in the brains of 5/8 mice following 10^5 PFU intranasal inoculation, we immunostained tissues for viral N protein at 4 and 6 dpi. We observed no antigen staining at 4 dpi (4/4 brains studied) but at 6 dpi saw extensive staining in several brain regions including the olfactory bulb, cerebral cortex, caudate/putamen, thalamus, hypothalamus, and ventral striatum (2/3 brains studied) (Extended Data Fig. 4a, Extended Data Table 1). Uninfected animals showed no N protein staining (3/3 mice). H&E staining demonstrated cell death and thrombi, noted in the thalamus (Extended Data Fig. 4b, c) and foci of cell death were sometimes also detected adjacent to degenerative ependyma cells (Extended Data Fig. 4d). The thalamus is affected in many COVID-19 patients with neurological disease[15]. Of note, while most of the affected areas are secondary or tertiary connections of the olfactory bulb, some, such as the area postrema and hypoglossal nucleus,

are not directly connected. Similar results were observed in analyses of SARS-CoV-infected mice[16]. These results suggest an important role for olfactory bulb infection in spread to the brain in some mice but also indicated that virus may enter the central nervous system by other routes. Infection of the olfactory epithelium is expected to precede brain infection and could also contribute to the anosmia and ageusia observed in many patients[1], including some who were asymptomatic or mildly symptomatic.

Infection of the sinonasal epithelium.

To assess virus replication in the upper respiratory tract following intranasal inoculation, we quantified viral RNA in nasal secretions by qRT PCR at 3 dpi. SARS-CoV-2 genomic RNA (C_t =21.5 +/−1.2 (mean +/− SEM)) was detected in secretions from 5 of 7 mice, and of these 5, 4 had evidence of subgenomic RNA (36.7 +/−1.1 (mean +/− SEM), consistent with active virus replication. Viral antigen was readily detected in both the respiratory and olfactory epithelium at 2 and 5 dpi. At 2 dpi virus antigen was present at multiple sites, often at the interface of the olfactory and respiratory epithelium (Fig. 1c). Viral antigen was also detected in nerve bundles subjacent to the olfactory epithelium (Extended Data Fig. 4e) and occasionally in vascular endothelia (Fig. 1d, left arrow) and Bowman's glands (Fig. 1d, right arrow). At sites of antigen positivity in the olfactory epithelium and maxillary sinus, we observed cell death and cellular debris at day 2 (Fig. 1e, f, Extended Data Fig. 4f), which progressed to cell sloughing and loss of cellularity by 5 dpi. (Fig. 1g, h). ACE2 has been detected in sustentacular cells in the olfactory epithelium[17], but not in olfactory sensory neurons, suggesting that these cells are a primary site of infection. Consistent with this, we detected SARS-CoV-2 antigen in sustentacular cells (Fig. 1i, j). Infection of sustentacular cells is not expected to result in spread to the olfactory bulb and its connections, but could still contribute to anosmia.

Anosmia in infected K-18-hACE2 mice.

To directly assess anosmia, we performed two sets of behavioral tests, both of which require a normal sense of smell, as described in Methods. First, in social scent discrimination assays, male mice were exposed to bedding containing female or male dander in a 2 ml Eppendorf tube (Fig. 2a). Mice identify the tube visually, and then preferentially spend time with the female dander, if olfaction is normal. Since female are not preferentially attracted to male dander[18], in a second experiment, female mice were exposed to bedding from their home cage ('familiar') and another, foreign cage ('novel') (Fig. 2d). Mice with normal olfaction preferentially explore the unfamiliar bedding. Third, we used a buried food test, in which mice are attracted to a food item hidden in the bedding that they were previously conditioned to detect (Fig. 2g). K18-hACE2 mice infected with SARS-CoV-2 did worse than controls in all the tests so that at days 2 and 3 p.i., male mice spent less time in the vicinity of the female dander (Fig. 2c), female mice were not attracted to the foreign bedding (Fig. 2f) and male and female mice took longer to find buried food (Fig. 2h, i). At 2 and 3 dpi, brains were not infected (Fig. 1b, Extended Data Fig. 4a) and mice exhibited minimal weight loss (Fig. 2b, e). Additionally, mobility was largely normal since there were no significant differences in the amount of time spent in exploring the tube containing male dander (Fig. 2c) or familiar bedding (Fig. 2f), when infected or uninfected mice were

compared. Preference indices were calculated for the social scent discrimination assays and confirmed hyposmia or anosmia (Extended Data Fig. 5). Together, these results suggest that hyposmia/anosmia at these times points is primarily caused by infection of the nasal epithelium and is not a consequence of generalized malaise or virus spread to the brain.

Human convalescent plasma therapy.

Convalescent plasma (CP) from COVID-19 survivors is being tested as a treatment in patients with clinical COVID-19[19]. Studies have demonstrated positive effects of CP on outcomes in several infectious diseases, if titers are sufficiently high and if CP is administered early in the disease course[20]. To assess the effect of CP on outcomes in SARS-CoV-2-infected K18-hACE2 mice, we administered undiluted and diluted human high titer plasma (neutralizing titer 1:1,480) intravenously 12 hours before infection. Undiluted plasma administered 12 hours before infection protected mice from death but not mild weight loss and reduced lung tissue titers while CP diluted 1:3 provided partial protection (Fig. 3a, b). Undiluted and diluted CP pretreatment markedly inhibited spread of infection to the brain (Fig. 3b) even in mice that died, supporting the conclusion that a lethal lung infection was the cause of death. On examination of lung tissues, levels of viral antigen and pathological changes were greatly decreased by CP treatment (Extended Data Fig. 6a). Delivery of undiluted plasma at 24 hrs post infection (p.i.) was partially protective (Extended Data Fig. 6b). Notably, CP did not diminish infection of sinonasal tissues (Fig. 3c). Finally, to assess the effects of CP treatment on SARS-CoV-2-induced anosmia, we treated infected mice with CP at 12 hours before infection and assessed mice for olfactory loss as described above (Fig. 2). Even though mice had minimal signs of clinical disease after CP treatment, by day 4 all mice exhibited profound anosmia (Fig. 2c, f, h, i, Extended Fig. 5).

DISCUSSION

SARS-CoV-2-infected K18-hACE2 mice developed dose-dependent lung disease with features similar to severe human COVID-19, including diffuse alveolar damage, inflammatory cell infiltration, tissue injury, lung vascular damage, and death. hACE2 transgenic mice driven by other promoters have also been developed, with variable outcomes observed after SARS-CoV-2 infection[21,22]. Remarkably, K18-hACE2 mice also support SARS-CoV-2 replication in the sinonasal epithelium and associated with this pathology develop anosmia, a common feature of human disease. Furthermore, the uniformly fatal disease outcome with a 10^5 inoculum was prevented by pre-treatment with CP from a COVID-19 patient. Notably, CP pre-treatment did not prevent initial infection of the lungs, damage to nasal respiratory and olfactory epithelia, or anosmia. We observed greater anosmia in female compared to male mice in the presence or absence of CP. Similarly, anosmia is more common in women compared to men with COVID-19[23-25]. SARS-CoV-2 infection of K18-hACE2 mice treated with CP or, potentially, neutralizing monoclonal antibodies will be especially useful for studies of anosmia because mice do not succumb to the infection, but like many infected patients with mild disease, have olfactory loss as a major manifestation[1]. Anosmia appears to result from initial infection and damage to supporting sustentacular cells and not to olfactory sensory neurons, suggesting that the

resulting inflammatory milieu, rather than direct neuronal damage is disease-causing. Therefore, we postulate that the observed anosmia has at least two possible, non-exclusionary explanations. First, the infection of sustentacular cells may disrupt signaling from olfactory sensory neurons (OSN) to the olfactory bulb. For example, sustentacular cells provide support to OSN by maintaining ion balance[26], which may be altered either directly by sustentacular cell infection or indirectly via disorganization of the olfactory epithelium (OE), leading to loss of cilia from OSN and deficient signal transduction[27,28]. The second possibility is collateral damage to OSN resulting from pro-inflammatory cytokine secretion by SARS-CoV-2-infected sustentacular cells. These cells have been reported to secrete cytokines such as TNF, Il-1β, Il-1α, and CXCL2 in chronic rhinosinusitis and COVID-19 patients[29,30]. Together, SARS-CoV-2-infected K18-hACE2 mice, readily available from Jackson Laboratories, recapitulate many of the finding observed in COVID-19 patients and provide a useful model to study pathogenesis and to evaluate interventions.

Online content.

Any methods, Nature Research reporting summaries, source data, extended data, supplementary information, acknowledgments, peer review information; details of author contributions and competing interests; and statements of data and code availability are available at https://doi.org/10.1038/s41586-020-2943-z.

METHODS

Human subjects approval.

Written informed consent was obtained from subjects to obtain plasma for participation in this study. The study was approved by the Institutional Review Board of the University of Iowa (IRB (#202003554 and #201402735).

Mice, cells, and virus.

Transgenic mice expressing human ACE2 were previously reported[4]. Human ACE2 is expressed under control of the cytokeratin 18 promoter. While the K18 promoter predominantly directs gene expression to multiple epithelia-lined tissues[8], it also directs reporter gene expression in neurons[31]. The mice (7-8 weeks old, male or female) used in these studies were obtained from the Jackson Laboratory (034860-B6.Cg-Tg(K18-ACE2)2Prlman/J) and are congenic on the C57BL/6 background. Non-transgenic C57BL/6 mice were used as controls in some experiments. All protocols were approved by the Institutional Animal Care and Use Committee of the University of Iowa. The 2019n-CoV/ USA-WA1/2019 strain of SARS-CoV-2 (Accession number: MT985325.1) used in these studies was passaged on Calu-3 2B4 cells (ATCC HTB-55). Calu-3 2B4 cells were grown in MEM (GIBCO, Grand Island, NY) supplemented with 20% FBS. Vero E6 cells (ATCC CRL-1586) were grown in Dulbecco's modified Eagle's medium (DMEM, GIBCO, Grand Island, NY) supplemented with 10% fetal bovine serum (FBS).

Infection of mice.

Mice were lightly anesthetized with ketamine/xylazine and infected intranasally with the indicated amount of SARS-CoV-2 in a total volume of 50 μl DMEM. Animal weight and

health were monitored daily. All experiments with SARS-CoV-2 were performed in a Biosafety Level 3 (BSL3) Laboratory at the University of Iowa.

Nasal lavage.—Mice were sedated with ketamine/xylazine (100 mg/kg ketamine/12.5 mg/kg xylazine). 100 µl of Carbachol (100 µg/ml) was administered I.P. and after approximately 15 minutes, nasal secretions were recovered. 20 µl secretions were recovered per mouse. Nasal secretions were immediately added to 500 µl Trizol, mixed and stored at −80°C until RNA was isolated.

Virus titer by plaque assay.

Virus or tissue homogenate supernatants were serially diluted in DMEM. 12 well plates of VeroE6 cells were inoculated at 37°C in 5% CO_2 for 1 h and gently rocked every 15 min. After removing the inocula, plates were overlaid with 0.6% agarose containing 2% FBS. After 3 days, overlays were removed, and plaques visualized by staining with 0.1% crystal violet. Viral titers were quantified as PFU/mL tissue.

Flow Cytometry.

The following monoclonal antibodies were used as described by manufacturer at a dilution of 1:200: anti-mouse CD3e-BV421 (clone 145-2C11, Cat. No.: 562600), anti-mouse CD16/32 (clone 93, Cat. No.:101302), anti-mouse CD4-PercP (clone RM4-5, Cat. No.: 550954), anti-mouse CD8-APC-Cy7 (clone 53-6.7, Cat. No.: 100714), anti-mouse CD220-APC (clone RA3-6B2, Cat. No.: 553092), anti-mouse Ly6C-PerCP (clone HK1.4, Cat. No.: 128028), anti-mouse Ly6G-FITC (clone 1A8, Cat. No.: 127606), anti-mouse CD11b-BV510 (clone M1/70, Cat. No.: 101263), anti-mouse CD11c-BV421 (clone N418, Cat. No.: 117343), anti-mouse CD64-PE-Cy7 (X54-5/7.1, Cat. No.: 139314), Biolegend, San Diego, CA; anti-mouse CD103-APC (clone 2E7, Cat. No.: 17-1031-80), anti-mouse TNF-FITC (clone MP6-XT22, Cat. No.: 11-7321-82), anti-mouse IFN-γ-APC (clone XMG1.2, Cat. No.: 25-7311-82), eBioscience, San Diego, CA. For intracellular cytokine staining (ICS), lymphocytes were cultured in 96-well dishes at 37°C for 5-6 h in the presence of 2 µM peptide pool and brefeldin A (BD Biosciences). Cells were then labeled for cell-surface markers, fixed/permeabilized with Cytofix/Cytoperm Solution (BD Biosciences), and labeled with anti-IFN-γ and anti-TNF antibody. All flow cytometry data were acquired using a BD FACSVerse and analyzed with FlowJo software.

Histology and Immunohistochemistry.

Animals were anesthetized and perfused transcardially with PBS, followed by zinc formalin. Lungs were fixed in zinc formalin. For routine histology, tissue sections (~4 µm each) were stained with hematoxylin and eosin. The following criteria were used for scoring edema, hyaline membrane formation and necrotic cellular debris: 0- none; 1-uncommon detection in <5% lung fields (200x); 2- detectable in up to 33% of lung fields; 3- detectable in up to 33-66% of lung fields; 4- detectable in >66% of lung fields. For scoring neutrophil infiltration: 0- within normal limits; 1-scattered PMNs sequestered in septa; 2- #1 plus solitary PMNs extravasated in airspaces; 3-#2 plus small aggregates in vessel and airspaces. For scoring mononuclear infiltrates, thrombosis and hemorrhage: 0-none; 1- uncommon

detection in <5% lung fields (200x); 2- detectable in up to 33% of lung fields; 3- detectable in up to 33-66% of lung fields; 4- detectable in >66% of lung fields.

For SARS-CoV-2 antigen detection, slides were incubated with blocking reagent (10% normal goat serum x 30 minutes) followed by rabbit monoclonal antibody against SARS-CoV2 N protein (1:20,000 dilution x 60 minutes, #40143-R019, Sino Biological US Inc., Wayne, PA, USA), then incubated with Rabbit Envision (Dako) and diaminobenzidine (Dako) as chromogen. Tissues were examined and scored in a post-examination method of masking by a boarded experimental pathologist[32]. Ordinal scores for lesion parameters were assigned using the following tiers: 0 = within expected limits; 1 - uncommon, <5%; 2 - detectable in 5-33%; 3 - detectable in 34-66% and 4 - detectable in >66% of lung fields (200x objective magnification).

Human convalescent plasma.

High titer convalescent plasma was collected with subject consent under an IRB (#202003554) approved protocol that allows use of samples for research. The convalescent plasma donor was a 58 year old female who had molecularly confirmed COVID-19 more than 4 weeks prior to their donation. Following the donation, she tested positive for HLA antibodies so the plasma was not eligible for administration to patients and was diverted to research. Antibody testing (EUROIMMUN SARS-COV-2 ELISA (IgG)) performed on this donor was 9.8, well above the cutoff of 1.1 for a positive result. Neutralization titer using a luciferase-expressing SARS-CoV-2 S protein pseudovirus assay showed that the neutralization IC_{50} titer was 1:1,480. Control plasma was obtained from an expired plasma unit collected prior to COVID-19 spread in our area and this product was collected under an IRB (#201402735) approved protocol that allows for research use of these products. Convalescent and control plasma were administered intravenously at the indicated times.

RNA isolation and qRT PCR.

Total RNA was extracted from tissues (or nasal lavage) using Trizol (Invitrogen) according to the manufacturer's protocol. Following a DNase treatment step 200 ng of total RNA was used as a template for first strand cDNA. The resulting cDNA was subjected to amplification of selected genes by real-time quantitative PCR using Power SYBR Green PCR Master Mix (Applied Biosystems). Average values from duplicates of each gene were used to calculate the relative abundance of transcripts normalized to HPRT and presented as 2^{-CT}. The primers used for cytokine and chemokines were previously reported[33]. For detection of viral genomes, the following primers were used to amplify the genomic RNA for the N protein: 2019-nCoV_N1-F: 5'-GAC CCC AAA ATC AGC GAA AT-3'; 2019-nCoV_N1-R: 5'-TCT GGT TAC TGC CAG TTG AAT CTG-3'. The following primers were used to amplify the subgenomic RNA for the E protein: F: 5'-CGATCTCTTGTAGATCTGTTCTC-3'; R: 5'-ATATTGCAGCAGTACGCACACA-3'.

Pseudovirus neutralizing antibody assay: To determine neutralization activity of patient and mouse plasma, we used a luciferase reporter-based pseudovirus neutralization assay, which has a nonreplicative vesicular stomatitis virus backbone coated with the SARS-CoV-2 spike protein. Sera from SARs-CoV-2-infected K18-hACE2 mice were collected at

the indicated time points and heat inactivated by incubation at 56°C for 30 min. Human convalescent plasma or mouse sera were serially diluted twofold in 96-well plates and incubated with the same volume of VSV pseudotyped with SARS-CoV-2 spike protein at 37°C for 1 h. Samples were placed onto Vero E6 cells and incubated at 37°C for 1 h to allow virus binding. After removal of the initial inoculum, cells were incubated for 24 hours. Neutralization was measured with a luciferase assay kit (Promega) and plotted relative to the value for control wells.

Behavioral studies.

Social Scent Discrimination Tests.

Male: Social-scent discrimination task was designed to assess the capability of mice to discriminate social scents as described previously[34]. Two identical tubes were separately sealed in a Ziploc bag in a large cage (used for housing rats (31 cm x 26 cm x 22 cm)) containing bedding from female mice and from the home (male) cage overnight. Next, SARS-CoV-2 infected or PBS-treated mice were released in a fresh cage containing the tubes placed at two different corners. Sniffing latency (sniffing and exploring the tubes) was calculated within a 5 min period. One trial on each mouse was performed each day with the position of tubes changed daily. Data were recorded in the BSL3 facility from a distance of approximately 1 meter.

Female: Two identical 3 cm dishes were separately sealed with mouse dander from the home cage ('familiar') and another cage ('novel') overnight. The dander-containing dishes were placed at two corners of a fresh cage. SARS-CoV-2 infected or PBS-treated mice were released into the cage and sniffing latency was calculated and recorded as described for male mice. One trial on each mouse was performed each day with the position of the dishes changed daily.

Preference index.: We calculated a preference index for each mouse, in order to compensate for any differences due to decreased mobility or malaise. The preference index for male mice is calculated as (female time - male time)/female time + male time) while for female mice, the preference index is (novel scent time – familiar scent time)/(novel scent time + familiar scent time). Data were analyzed using Mann-Whitney U-tests.

Buried Food Test: Evaluation of odor detection was carried out by a buried food test as described previously[34]. Briefly, food palatability was confirmed prior to initiation of the experiments. SARS-CoV-2 infected or PBS-treated mice were sensitized to the food for 10-15 minutes on the day of the experiment. The food pellet was then buried approximately 1 cm below the surface of bedding in a fresh cage. One trial per infected or mouse per day was performed with the position of the food changed on a daily basis. The latency to locate and uncover the buried food pellet was recorded with a stopwatch. Mice were allowed to explore the cage for 4 min and if they could not locate the food, the time was recorded as 4 min. The experiment was repeated daily.

Statistical analysis.

Differences in mean values between groups were analyzed by ANOVA and Student's t tests and differences in survival were analyzed by log-rank (Mantel-Cox) tests using GraphPad Prism 8. All results are expressed as mean ± standard error (SEM) and were corrected for multiple comparisons. For behavioral studies, data from the social scent discrimination tests, and buried food test were analyzed by two-way ANOVA and nonparametric (Mann-Whitney *U*-tests) tests, respectively. *P* values of <0.05 were considered statistically significant. (*, *P* values of 0.05. **, P values of 0.005. ***, *P* values of 0.0005. ****, *P* values of 0.0001).
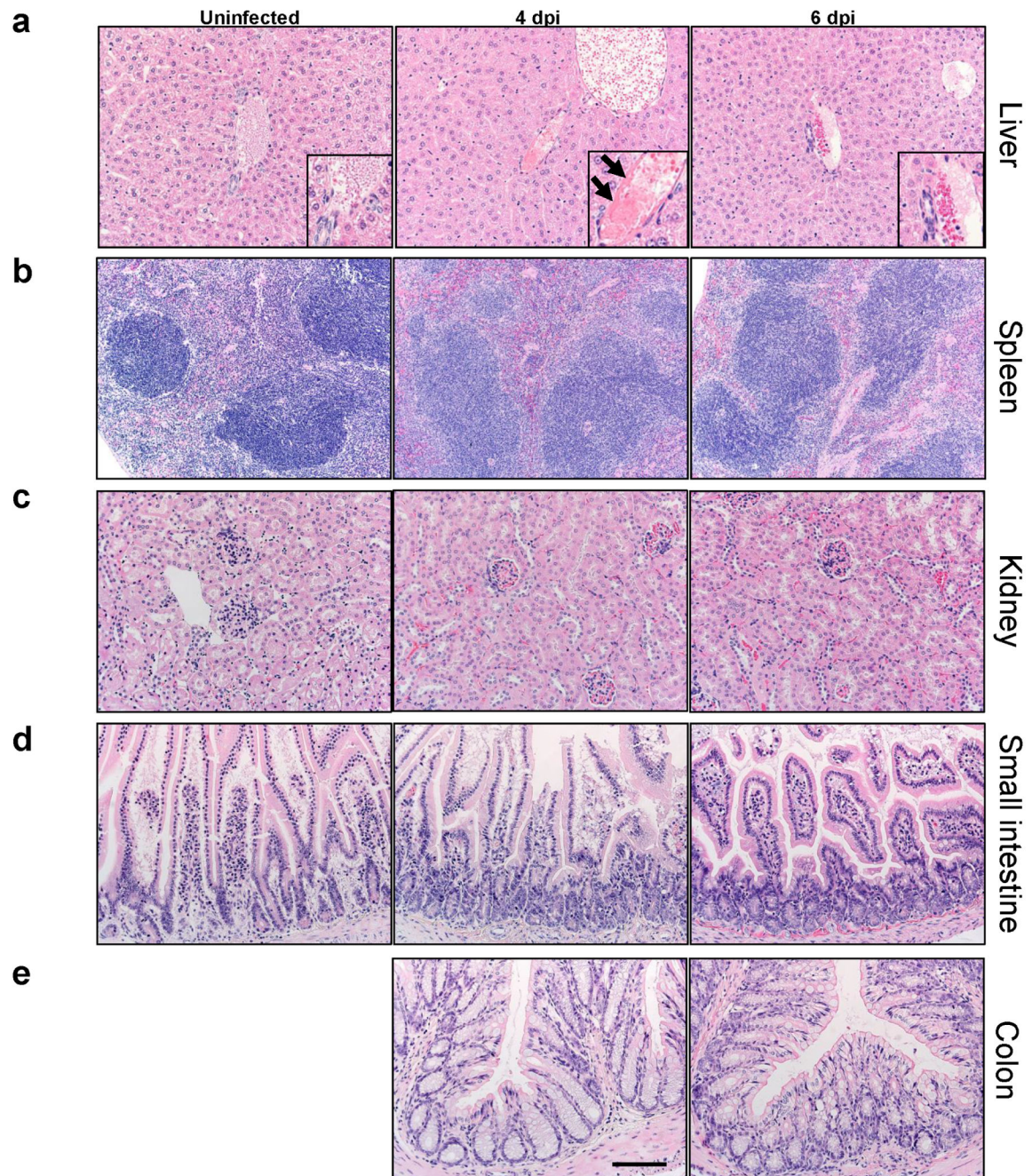
Extended Data
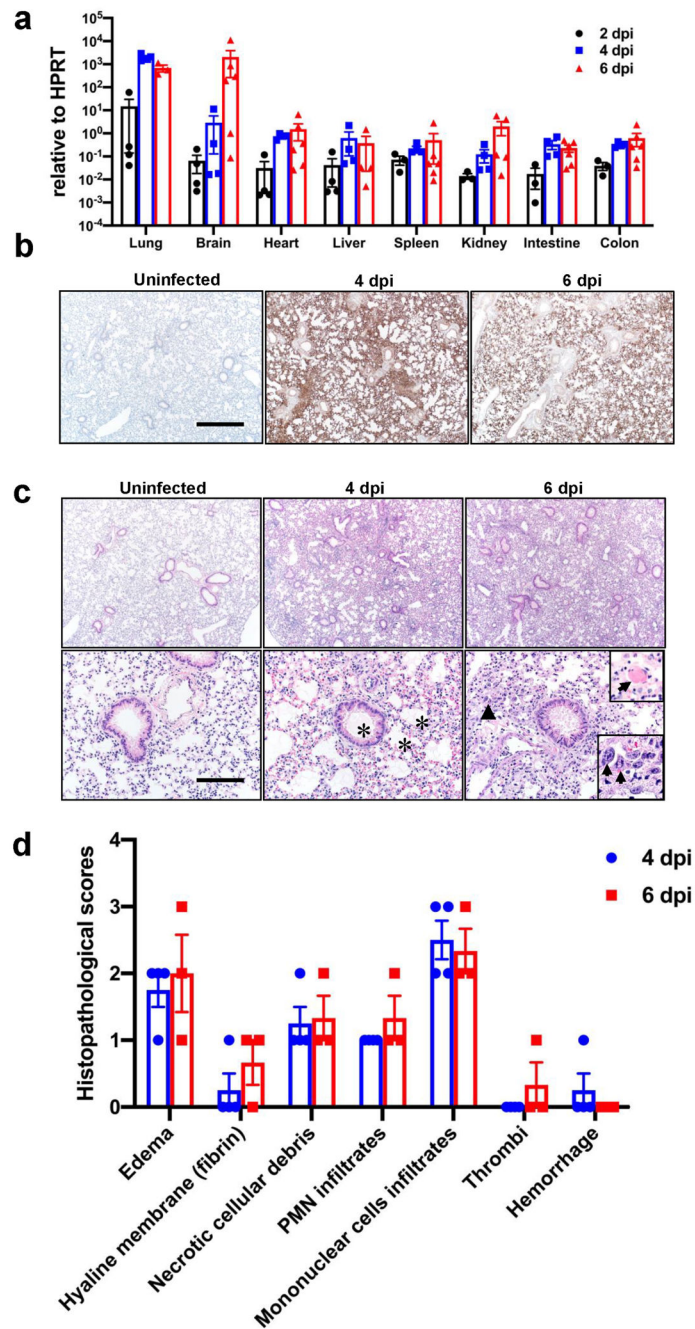
**Extended Data Fig. 1. Clinical and pathological disease in SARS-CoV-2-infected K18-hACE2 mice.**

Mice were infected intranasally with 10^5 PFU SARS-CoV-2. a. Viral RNA detected by qPCR targeting viral N gene with normalization to HPRT for the indicated organs at 2, 4, and 6 dpi (10^3, n=4; 10^4, n=4; 10^5, n=6, each organ was collected from an individual mouse). b. Lungs from uninfected (n=3), and infected (day 4 (n=4) and day 6 (n=3) p.i.) mice were immunostained to detect SARS-CoV-2 N protein. Bar = 701 μm. c. Infected lungs

exhibited evidence of airway edema (asterisks, bottom middle panel), alveolar hyaline membranes, vascular thrombosis (upper inset and arrow, bottom right panel), dying cells with pyknotic to karyorrhectic nuclei, and proliferative alveolar epithelium (arrowhead and lower inset, bottom right panel, arrows) Bar = 701 and 70 μm (top and bottom, respectively), H&E stain. d. Summary of lung lesion scoring, as described in Methods (uninfected, n=3; day 4, n=4; day 6, n=3, each brain was collected from an individual mouse). Two sections of each lung from 3-4 mice per group were evaluated. These data are representative of 3 independent experiments. (a, d). Data are shown as mean±SEM.

**Extended Data Fig. 2. Histological analysis of extrapulmonary tissue.**
Mice were sacrificed at days 0, 4 and 6 p.i. with 10^5 PFU SARS-CoV-2 and tissues prepared
for histological examination. Liver (a), spleen (b), kidney (c), small intestine (d), and colon
(e) were studied. Pathological changes were minor and only observed in the liver. In the
liver, all mice had some blood vessels filled with clear space or aggregates variably
composed of erythrocytes / platelets (insets). Rare vessels had evidence of eosinophilic
fibrillar material adherent along the vascular wall consistent with fibrin thrombi (a, arrows,
inset, middle panel) adherent along the vascular wall. Bar = 110 (a,c-e) and 221 μm (b),
H&E stain. Two sections of each organ from 3-4 mice per group were evaluated.
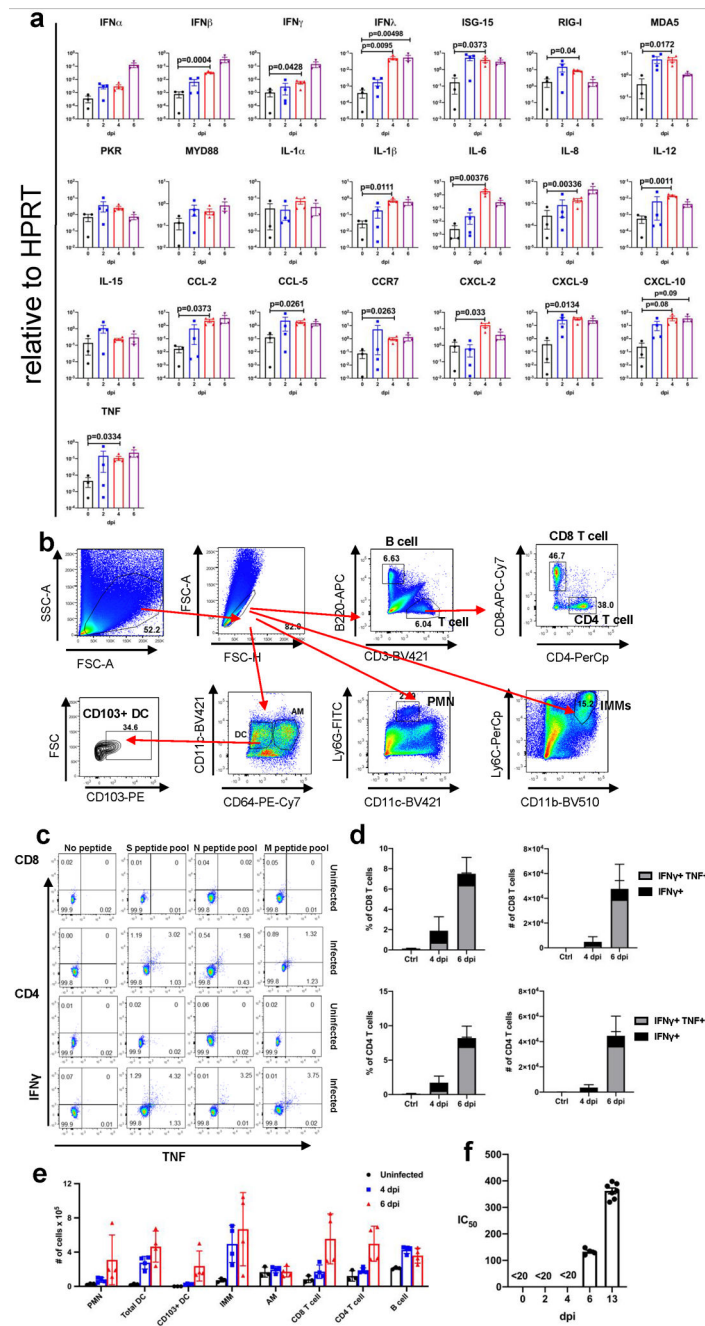
Extended Data Fig. 3. Inflammatory mediators and immune effector cells in infected lungs.
a. Cytokine and chemokine transcripts were measured by qPCR following reverse transcription of RNA isolated from the lungs of K18-hACE2 mice infected with 10^5 PFU SARS-CoV-2 (mock and 6 dpi, n=3; 2 and 4 dpi, n=4, each lung was collected from an individual mouse), one independent experiment. Statistical significance compared to results obtained at 0 dpi. Data were analyzed using 2-tailed Student's t tests without adjustments. b. Gating strategy for identification of immune cells in lungs is shown. c. Representative FACS plot of IFNγ⁺TNF⁺ CD8 and CD4 T cells (as gated in panel b) after stimulation with indicated peptide pools in the lungs of 10^5 PFU SARS-CoV-2 infected K18-hACE2 mice. d.

Summary data are shown (n=3 mice/time point). Data are representative of two independent experiments e. Quantification of immune cells (as gated in panel b) in the lungs (n=3 for uninfected group; n=4 for 4 and 6 dpi, each lung was collected from an individual mouse). Data are representative of two independent experiments. f. Sera were collected from infected mice at the indicated time points and IC_{50} values determined by neutralization of SARS-CoV-2 pseudoviruses expressing luciferase (n=4, days 0,2,4,6; n=7, day 13, 2 independent experiments). (a, d-f) Data are shown as mean±SEM.
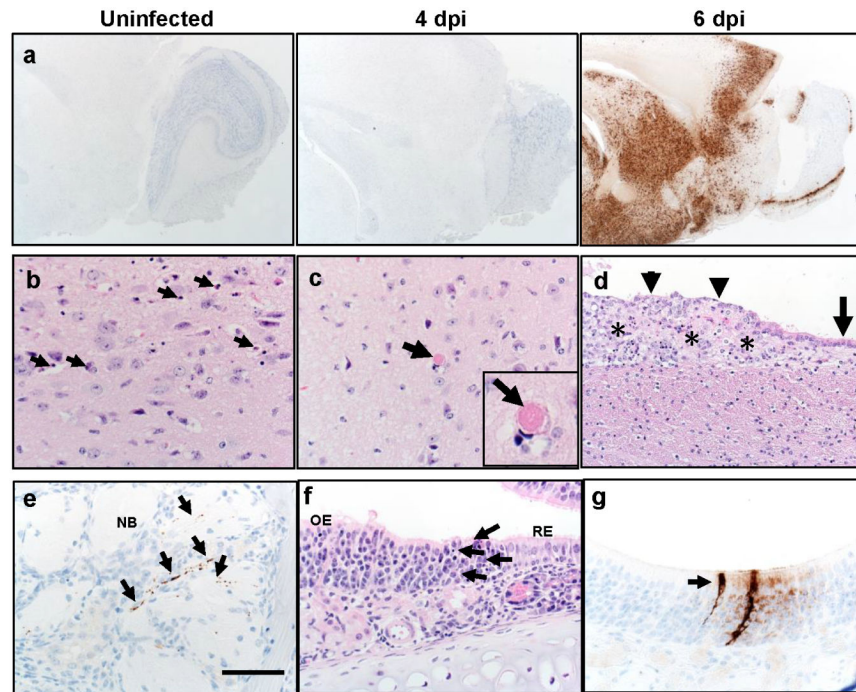

Extended Data Fig. 4. Brain and nasal cavity infection in SARS-CoV-2 infected K18-hACE2 mice.
a. Brains from uninfected and infected (10^5 PFU SARS-CoV-2) mice were immunostained to detect SARS-CoV-2 N protein b, c. Multiple sites were characterized by cellular and karyorrhectic nuclear debris (b, arrows). Thrombi were detected, seen here in thalamus (c, arrow and inset). Bar = 17 μm. d. Ependyma (arrow) at day 6 p.i. had focal denudation and degeneration of ependymal cells (arrowheads) overlying focal region of cellular and karyorrhectic nuclei debris (asterisks). e. Nerve bundles (NB) subjacent to OE had evidence of punctate to linear immunostaining (brown, arrows). f. Sites of N protein localization at interface of OE and RE at day 2 p.i. (see Fig. 1d) had evidence of cell death and cellular debris (arrows). g. OE with sustentacular cell immunostaining for N protein. Bar = 1.3 mm (a), 65 μm (b,c,e-g) and 130 μm (d). Two sections of each tissue from 3-4 mice per group were evaluated.
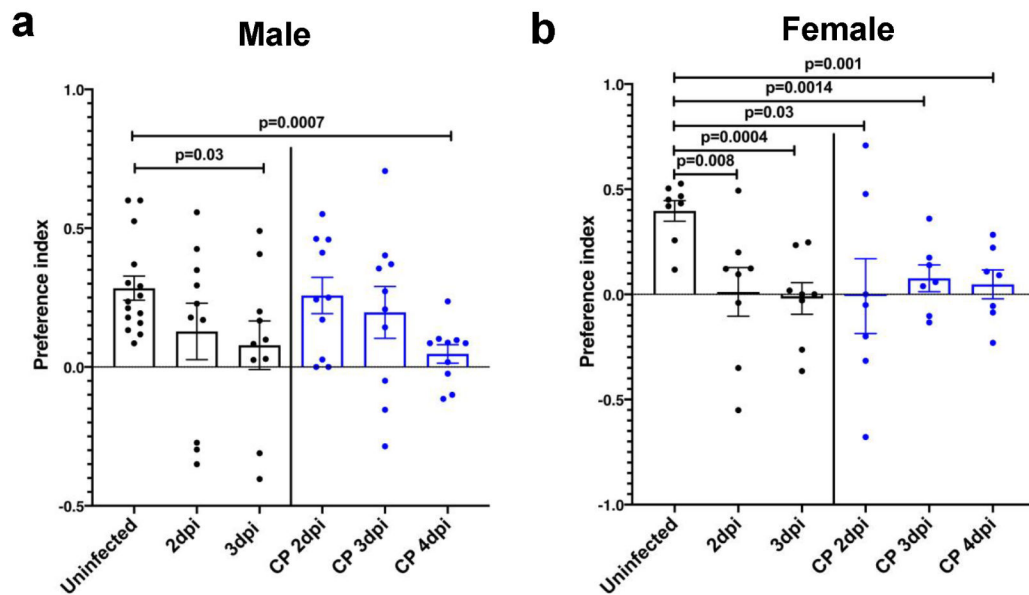
Extended Data Fig. 5. Preference indices for social scent discrimination assays.
Preferences indices were calculated as described in Methods for each mouse shown in
Figure 2. The preference index was calculated as time spent with preferred or nonpreferred
scent: (preferred - nonpreferred) / (preferred + non preferred). a. For male mice, preferred
scent = female dander; non preferred = male dander; (uninfected: n=15 mice, other groups:
n=10 mice). b. For female mice, preferred scent = novel scent; nonpreferred = familiar scent;
(uninfected and infected alone groups: n=8 mice each; infected/CP-treated groups: n=7
mice). Data were analyzed for statistical significance using 2-tailed Mann-Whitney *U*-tests
and shown as mean±SEM.
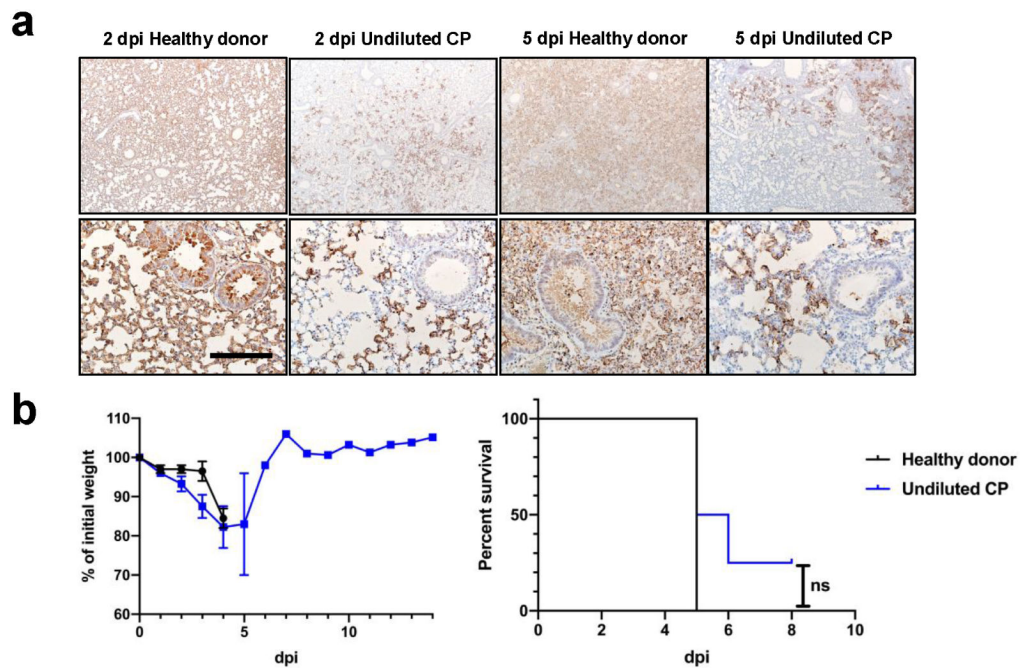
Extended Data Fig. 6. Effects of Convalescent plasma delivered 6 hours before or 24 hours after infection.

a. N protein immunostaining in the lungs of control (healthy donor) plasma or convalescent plasma (CP)-treated mice at 2 and 5 days p.i. with 10^5 PFU SARS-CoV-2. Bar = 800 μm (top) and 160 μm (bottom). Two sections of each lung from 3 mice per group evaluated. Representative images are shown. b. Percentage of initial weight (left panel), and survival (right panel) of K18-hACE2 mice receiving control plasma (n=2) or undiluted CP (n=4) at 24 hours after challenge with 10^5 PFU SARS-CoV-2. Data are shown as mean±SEM and are representative of one independent experiment. ANOVA and 2-tailed Student's t tests without adjustments (weights) and log-rank (Mantel-Cox) tests (survival) were used to analyze these data.

Supplementary Material

Refer to Web version on PubMed Central for supplementary material.

ACKNOWLEDGMENTS

DATA AVAILABILITY.

The data supporting the findings of this study are documented within the paper and are available from the corresponding authors upon request.

REFERENCES

1. Spinato G et al. Alterations in Smell or Taste in Mildly Symptomatic Outpatients With SARS-CoV-2 Infection. JAMA, doi:10.1001/jama.2020.6771 (2020).

2. Williamson EJ et al. Factors associated with COVID-19-related death using OpenSAFELY. Nature 584, 430–436, doi:10.1038/s41586-020-2521-4 (2020). [PubMed: 32640463]

3. Munoz-Fontela C et al. Animal models for COVID-19. Nature, doi:10.1038/s41586-020-2787-6 (2020).

4. McCray PB Jr. et al. Lethal infection in K18-hACE2 mice infected with SARS-CoV. J Virol 81, 813–821 (2006). [PubMed: 17079315]

5. Zhou P et al. A pneumonia outbreak associated with a new coronavirus of probable bat origin. Nature 579, 270–273, doi:10.1038/s41586-020-2012-7 (2020). [PubMed: 32015507]

6. Tseng CT et al. SARS coronavirus infection of mice transgenic for the human angiotensin-converting enzyme 2 (hACE2) virus receptor. J Virol 81, 1162–1173 (2006). [PubMed: 17108019]

7. Yang XH et al. Mice transgenic for human angiotensin-converting enzyme 2 provide a model for SARS coronavirus infection. Comp Med 57, 450–459 (2007). [PubMed: 17974127]

8. Chow YH et al. Development of an epithelium-specific expression cassette with human DNA regulatory elements for transgene expression in lung airways. Proc Natl Acad Sci U S A 94, 14695–14700 (1997). [PubMed: 9405675]

9. Ackermann M et al. Pulmonary Vascular Endothelialitis, Thrombosis, and Angiogenesis in Covid-19. N Engl J Med 383, 120–128, doi:10.1056/NEJMoa2015432 (2020). [PubMed: 32437596]

10. Feldstein LR et al. Multisystem Inflammatory Syndrome in U.S. Children and Adolescents. N Engl J Med 383, 334–346, doi:10.1056/NEJMoa2021680 (2020). [PubMed: 32598831]

11. Winkler ES et al. SARS-CoV-2 infection of human ACE2-transgenic mice causes severe lung inflammation and impaired function. Nat Immunol, doi:10.1038/s41590-020-0778-2 (2020).

12. Bradley BT et al. Histopathology and ultrastructural findings of fatal COVID-19 infections in Washington State: a case series. Lancet 396, 320–332, doi:10.1016/S0140-6736(20)31305-2 (2020). [PubMed: 32682491]

13. Mathew D et al. Deep immune profiling of COVID-19 patients reveals distinct immunotypes with therapeutic implications. Science 369, doi:10.1126/science.abc8511 (2020).

14. Channappanavar R et al. Dysregulated type I interferon and inflammatory monocyte-macrophage responses cause lethal pneumonia in SARS-CoV-infected mice. Cell Host Microbe 19, 181–193, doi:10.1016/j.chom.2016.01.007 (2016). [PubMed: 26867177]

15. Poyiadji N et al. COVID-19-associated Acute Hemorrhagic Necrotizing Encephalopathy: Imaging Features. Radiology 296, E119–E120, doi:10.1148/radiol.2020201187 (2020). [PubMed: 32228363]

16. Netland J, Meyerholz DK, Moore S, Cassell M & Perlman S Severe acute respiratory syndrome coronavirus infection causes neuronal death in the absence of encephalitis in mice transgenic for human ACE2. J Virol 82, 7264–7275 (2008). [PubMed: 18495771]

17. Bilinska K, Jakubowska P, Von Bartheld CS & Butowt R Expression of the SARS-CoV-2 Entry Proteins, ACE2 and TMPRSS2, in Cells of the Olfactory Epithelium: Identification of Cell Types and Trends with Age. ACS Chem Neurosci 11, 1555–1562, doi:10.1021/acschemneuro.0c00210 (2020). [PubMed: 32379417]

18. Dey S et al. Cyclic Regulation of Sensory Perception by a Female Hormone Alters Behavior. Cell 161, 1334–1344, doi:10.1016/j.cell.2015.04.052 (2015). [PubMed: 26046438]

19. Joyner MJ et al. Early safety indicators of COVID-19 convalescent plasma in 5,000 patients. J Clin Invest, doi:10.1172/JCI140200 (2020).

20. Casadevall A, Joyner MJ & Pirofski LA SARS-CoV-2 viral load and antibody responses: the case for convalescent plasma therapy. J Clin Invest, doi:10.1172/JCI139760 (2020).

21. Bao L et al. The pathogenicity of SARS-CoV-2 in hACE2 transgenic mice. Nature 583, 830–833, doi:10.1038/s41586-020-2312-y (2020). [PubMed: 32380511]

22. Jiang RD et al. Pathogenesis of SARS-CoV-2 in Transgenic Mice Expressing Human Angiotensin-Converting Enzyme 2. Cell 182, 50–58 e58, doi:10.1016/j.cell.2020.05.027 (2020). [PubMed: 32516571]

23. Makaronidis J et al. Seroprevalence of SARS-CoV-2 antibodies in people with an acute loss in their sense of smell and/or taste in a community-based population in London, UK: An observational cohort study. PLoS Med 17, e1003358, doi:10.1371/journal.pmed.1003358 (2020). [PubMed: 33001967]

24. Giacomelli A et al. Self-reported Olfactory and Taste Disorders in Patients With Severe Acute Respiratory Coronavirus 2 Infection: A Cross-sectional Study. Clin Infect Dis 71, 889–890, doi:10.1093/cid/ciaa330 (2020). [PubMed: 32215618]

25. Lechien JR et al. Olfactory and gustatory dysfunctions as a clinical presentation of mild-to-moderate forms of the coronavirus disease (COVID-19): a multicenter European study. Eur Arch Otorhinolaryngol 277, 2251–2261, doi:10.1007/s00405-020-05965-1 (2020). [PubMed: 32253535]

26. Vogalis F, Hegg CC & Lucero MT Ionic conductances in sustentacular cells of the mouse olfactory epithelium. J Physiol 562, 785–799, doi:10.1113/jphysiol.2004.079228 (2005). [PubMed: 15611020]

27. Bryche B et al. Massive transient damage of the olfactory epithelium associated with infection of sustentacular cells by SARS-CoV-2 in golden Syrian hamsters. Brain Behav Immun, doi:10.1016/j.bbi.2020.06.032 (2020).

28. Zhang AJ et al. SARS-CoV-2 infects and damages the mature and immature olfactory sensory neurons of hamsters. Clin Infect Dis, doi:10.1093/cid/ciaa995 (2020).

29. Imamura F & Hasegawa-Ishii S Environmental Toxicants-Induced Immune Responses in the Olfactory Mucosa. Front Immunol 7, 475, doi:10.3389/fimmu.2016.00475 (2016). [PubMed: 27867383]

30. Torabi A et al. Proinflammatory Cytokines in the Olfactory Mucosa Result in COVID-19 Induced Anosmia. ACS Chem Neurosci 11, 1909–1913, doi:10.1021/acschemneuro.0c00249 (2020). [PubMed: 32525657]

Extended data references

31. Chow YH et al. Targeting transgene expression to airway epithelia and submucosal glands, prominent sites of human CFTR expression. Mol Ther 2, 359–367, doi:10.1006/mthe.2000.0135 (2000). [PubMed: 11020351]

32. Meyerholz DK & Beck AP Principles and approaches for reproducible scoring of tissue stains in research. Lab Invest 98, 844–855, doi:10.1038/s41374-018-0057-0 (2018). [PubMed: 29849125]

33. Li K et al. Middle East Respiratory Syndrome Coronavirus Causes Multiple Organ Damage and Lethal Disease in Mice Transgenic for Human Dipeptidyl Peptidase 4. J Infect Dis 213, 712–722, doi:10.1093/infdis/jiv499 (2016). [PubMed: 26486634]

34. Yang M & Crawley JN Simple behavioral assessment of mouse olfaction. Curr Protoc Neurosci **Chapter 8**, Unit 8 24, doi:10.1002/0471142301.ns0824s48 (2009)**Chapter 8**
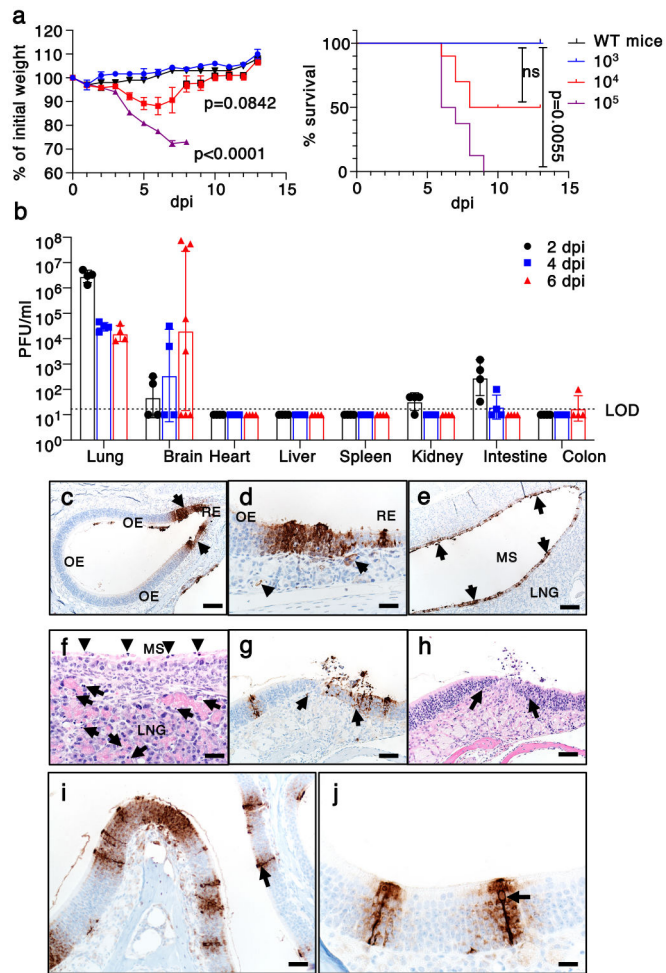
Fig. 1. Clinical and pathological disease in SARS-CoV-2-infected K18-hACE2 mice.
a. Percentage of initial weight and survival of wild type (n=1 mouse) and K18-hACE2 mice infected with 10^3 (n=3 mice), 10^4 (n=10 mice), or 10^5 (n=8 mice) PFU SARS-CoV-2/mouse (2 independent experiments). ANOVA and 2-tailed Student's t tests without adjustments (weight change) and log-rank (Mantel-Cox) tests (survival) were used to analyze these data. Left panel, P<0.0001 10^3 vs 10^5 PFU inoculum; p=0.0842 for 10^4 vs 10^5 PFU inoculum. b. Infectious virus titers detected by plaque assay in different organs at 2, 4, and 6 dpi with 10^5 PFU SARS-CoV-2 (day 2, 4 n=4 mice; day 6, n=8 mice (brain) and n=4 (other organs). 3 independent experiments). LOD=limit of detection. c-j. Nasal and sinus tissue were examined at days 2 (c-f) and 5 (g-j). N protein immunostaining (c,d,e,g,i,j) and H&E stain (f,h). (a,b) Data are shown as mean±SEM. c. N protein immunostaining in olfactory epithelium (OE). d. N protein immunostaining (brown) localized near interface of OE and respiratory epithelium (RE). Subjacent to epithelium, N protein was occasionally detected in endothelial lining of vessels (left arrow) and Bowman's glands (right arrow) were occasionally detected. e-f. Maxillary sinus (MS) lining epithelium had extensive immunostaining for N protein (e, brown, arrows) with common sloughing and cellular debris (f, arrowheads). The lateral nasal glands (LNG) also had multifocal cellular and karyorrhectic debris (f, arrows). g-h. OE at day 5 with N protein immunostaining (g, arrows)

localized near interface with respiratory epithelium. At these sites, cellular sloughing and loss of cellularity (h, arrows) were seen. i-j. Strong N protein immunostaining (arrows) was seen in tall OE cells with "classic" morphology of sustentacular cells along with immunostain expanding to adjacent cells. Bars = 128 (c,e), 63 (g,h), 31 (d,f), 42 (i), and 21 (j) μm, respectively. Two sections of each tissue from 3-4 mice per group were evaluated.
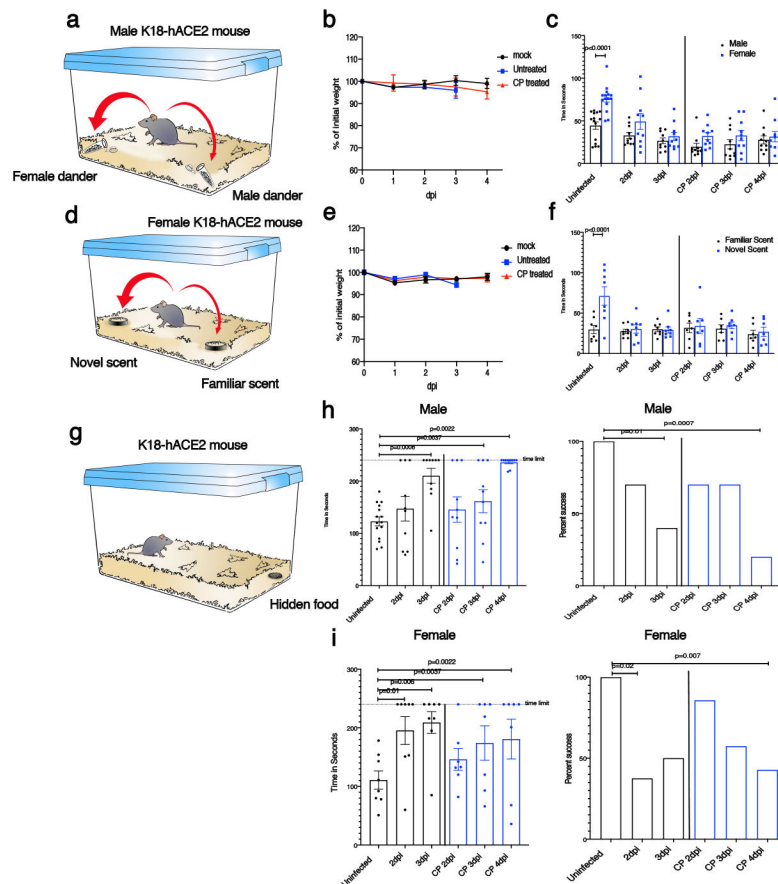
Fig. 2. SARS-CoV-2 infection causes anosmia in K18-hACE2 mice.

Male and female mice were treated with PBS (uninfected) or 10^5 PFU SARS-CoV-2 intranasally. a,d. Schematic showing social scent discrimination tests. b,e. Weights were recorded daily. c. Each male mouse was allowed 5 minutes in the cage with male and female scent (bedding from male or female cages) placed at two corners of the cage. The time that male mice spent sniffing male or female scent was recorded. Data were analyzed by 2-way ANOVA. f. Female mice were exposed to their own bedding ('familiar') or bedding from another cage ('novel'). The time that female mice spent exploring each bedding was recorded. Data were analyzed by 2-way ANOVA. In some experiments, mice were pretreated with undiluted convalescent plasma (results on right of vertical line (c,f)). g-i. Buried food test (schematic shown in g). Food was buried under the bedding and each mouse was allowed 4 minutes in the cage to search for the food. h. The dotted line denotes the time limit of 4 minutes. Data were analyzed by 2-tailed Mann-Whitney U-tests. i. The percentage of mice that found the buried food within 4 minutes is shown. Data were analyzed by χ^2 Fisher's exact test. In some experiments, mice were pretreated with undiluted convalescent plasma (denoted by blue bars in h,i). Male mice: uninfected: n=15 mice; infected: n=10 mice. Female mice: uninfected and infected: n=8 mice each; infected/CP-treated: n=7 mice. analyzed in 4 independent experiments. (b,c,e,f,h,i) Data are shown as mean±SEM. Preferences indices for the social scent discrimination assays are shown in Extended Data 5.
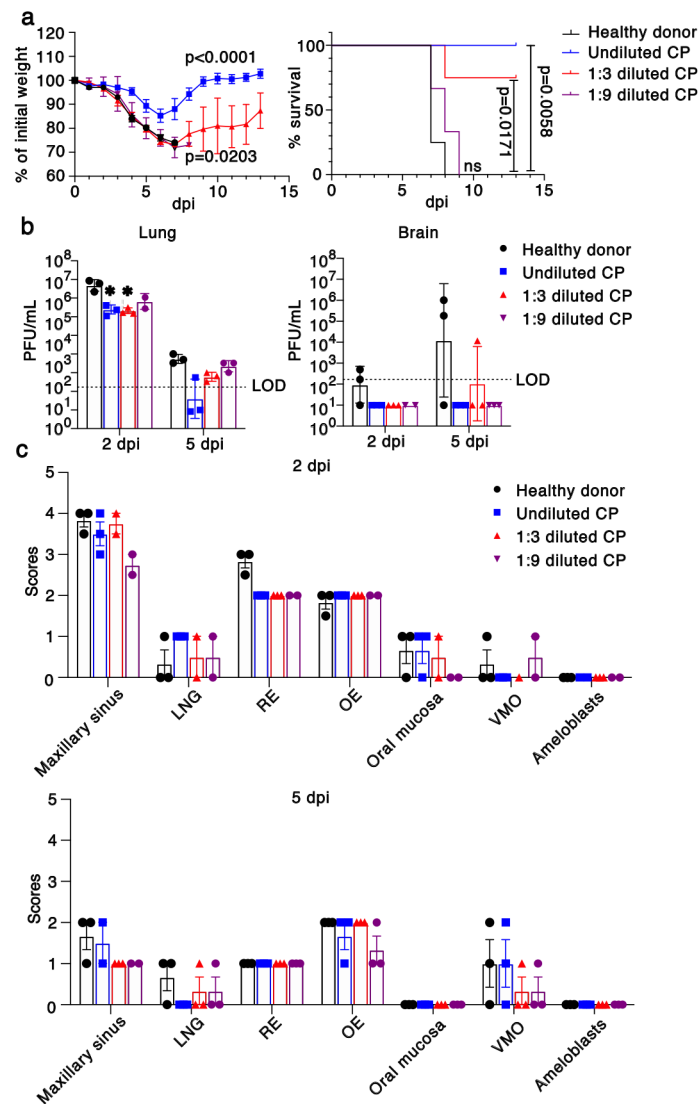
Fig. 3. Effects of convalescent plasma (CP) on outcomes.

a. Percentage of initial weight (left panel) and survival (right panel) of K18-hACE2 mice receiving control serum (n=4 mice, black), undiluted (n=4 mice, blue), 1:3 dilution (n=4 mice, red) and 1:9 dilution (n=3 mice, purple) human CP at 24 hours prior to challenge with 10^5 PFU SARS-CoV-2. Data are from two independent experiments. ANOVA and 2-tailed Student's t tests without adjustments (weight change) and log-rank (Mantel-Cox) tests (survival) were used to analyze these data. b. Viral titers of CP-treated mice in the lungs (left panel) and brains (right panel) at 2 and 5 dpi. n=3 except for 2 dpi, 1:9 dilution (n=2) mice, 1 independent experiment. LOD=limit of detection. 2-tailed Student's t tests without adjustments were used to analyze these data. * P=0.0455, control vs. undiluted CP; P=0.0443 control vs. 1:3 diluted CP. c. Scores of N protein immunostaining in CP-treated mice in the nasal cavity at 2 (upper panel) and 5 (lower panel) dpi. 0 – none; 1 - rare <1%; 2 - multifocal or localized <33% cells; 3 - multifocal, coalescing, 33-66%; 4 - extensive >67%. Two sections of each sinonasal cavity from three mice per group were evaluated.

Data are shown as mean±SEM. LNG-lateral nasal gland, RE-respiratory epithelium, OE-olfactory epithelium, VMO-vomeronasal organ.

Extended Data Table 1.
Distribution of SARS-CoV2 antigen in Brain.

4 brains were analyzed at 6dpi. + <++<+++ Represents Relative density of antigen presence. - No antigen detected. (+) Represents presence of antigen in some samples only. AON-Anterior Olfactory Nucleus. Neuroanatomical Reference: ALLEN Brain Atlas. http://atlas.brain-map.org/atlas?atlas=2#atlas=2&plate=100883770&structure=168&x=7797.5&y=4023.9999997615814&zoom=−3&resolution=10.47&z=5.

Olfactory Bulb		Thalamus	
Main Olfactory Bulb		Ventral Posterolateral Nucleus	+++
Glomerular Layer	−	Ventral Posteromedial Nucleus	+++
Granule Layer	−	Ventral Medial Nucleus	++
Inner Plexiform Layer	−	Ventral Anterior-Lateral Complex	+++
Mitral Layer	+	Anterior group of the Dorsal Thalamus	+++
Outer Plexiform Layer	−	Medial group of the Dorsal Thalamus	+++
		Midline group of the Dorsal Thalamus	+++
Accessory Olfactory Bulb		Reticular Nucleus	+++
Glomerular Layer	−	Geniculate Group	+++
Granular Layer	−		
Mitral Layer	++	**Hypothalamus**	+++
		Supraoptic Nucleus	+++
AON Dorsal	+++	Paraventricular Nucleus	+++
AON Medial	++	Arcuate Nucleus	+++
AON lateral	++	Suprachiasmatic Nucleus	+++
Taenia Tecta	+	Subfornical Organ	+++
		Anterior Nucleus	+++
		Premammillary Nucleus	+++
Midbrain		**Hind Brain**	
Superior Colliculus	++	Pons	
Inferior Colliculus	++	Nucleus of Lateral Lemniscus	++
Nucleus Brachium	++	Trigeminal Nucleus	++
Nucleus Sagulum	++	Parabrachial Nucleus	++
Para Bigeminal Nucleus	++	Dorsal Tegmental Nucleus	++
Midbrain Trigeminal Nucleus	++	Pontine Nuclei	++
Substantia Nigra	+++	Supratrigeminal Nucleus	++
Ventral Tegmental Area	++	Superior Central Nucleus Raphe	++
Reticular Nucleus	+++	Locus Ceruleus	++
Cuneiform Nucleus	++	Laterodorsal Tegmental Nucleus	++
Red Nucleus	++		
Oculomotor Nucleus III	++	Medulla	
Edinger-Westphal Nucleus	++	Area Postrema	+++
Trochlear Nucleus IV	++	Cochlear Nuclei	++
Ventral Tegmental Nucleus	++	Dorsal Column Nuclei	++

Olfactory Bulb		Thalamus	
Pedunculopontine Nucleus	++	External Cuneate Nucleus	+
		Nucleus Ambiguus	++
		Solitary Tract Nucleus	++
		Lateral Reticular Nucleus	++
		Magnocellular Reticular Nucleus	++
		Medullary Reticular Nucleus	++
		Parvicellular Reticular Nucleus	++
		Nucleus X	++
		Hypoglossal Nucleus XII	++
Hippocampus	(+)		
Cerebellum	−		